In field Vis/NIR hyperspectral imaging to measure soluble solids content of wine grape barriers during ripening

In-field Vis/NIR hyperspectral imaging to measure soluble solids content of wine grape berries during ripening

Alessandro Benelli
Department of Agricultural and Food Sciences
Alma Mater Studiorum, University of Bologna
Cesena, Italy
alessandro.benelli6@unibo.it

Chiara Cevoli
Department of Agricultural and Food Sciences
Alma Mater Studiorum, University of Bologna
Cesena, Italy
chiara.cevoli3@unibo.it

Angelo Fabbri
Department of Agricultural and Food Sciences
Alma Mater Studiorum, University of Bologna
Cesena, Italy
angelo.fabbri@unibo.it

***Abstract*—Monitoring the quality attributes of grapes is a practice that allows to check the grapes' state of ripeness and to decide when it is appropriate to proceed with the harvest. In the present study, a non-destructive method based on hyperspectral imaging (HSI) technology was developed. Analyses were carried out directly in the field using a Vis/NIR (400–1000 nm) hyperspectral camera (HSC) between the rows of 'Sangiovese' (*Vitis vinifera* L.) vineyard destined for wine production. One vineyard row was analyzed on 13 different days. During the trials, 33 berries were collected and the soluble solids content (SSC) expressed in terms of °Brix (°Bx) was measured by a portable digital refractometer. The mean spectra of the selected berries were extracted from each hyperspectral (HS) image. The pre-treated mean spectra were used to predict the SSC of the berries by means of partial least squares (PLS) regression, obtaining a value of $R^2 = 0.75$ in cross-validation, with RMSECV = 0.84 °Bx. The present study shows the potential of the use of HSI technology directly in the field through proximal measurements under natural light conditions for the prediction of the SSC quality attribute of grapes.**

Keywords—hyperspectral, in-field, grape, wine, soluble solids content, classification, prediction

I. Introduction

Italy is the largest wine producer in the world, with a production in 2018 of 54.8 million hL (18.8% of world production) [1]. In an industrialized wine growing system, monitoring the quality attributes of grapes is extremely important: well-planned monitoring allows to check the growth and ripening of the grapes, and finally to decide when to proceed with the harvest. In this way, the prerequisites for obtaining a high-quality wine are established, with the consequent economic and social impact.

The combination of new sensor, navigation and satellite positioning technologies adopted in order to monitor and optimize wine production processes, are the basis of the concept of precision viticulture (PV), which derives from precision agriculture (PA) or precision farming. PA is a relatively recent agricultural development model, introduced in the mid-1980s: thanks to PA's own methods it is possible to increase the quantity and quality of agricultural production by reducing inputs (water, energy, fertilizers, pesticides, etc.). The objectives are the reduction of production costs, environmental impact and the increase of production, improving its quality [2], [3]. PV was first applied in the middle of the first decade of the 2000s.

The most recent studies related to PV have largely made use of unmanned aerial vehicles (UAV), due to reduced operating costs, greater flexibility of use and spatial imagery resolution than traditional aircraft or satellite based technologies [4]. Several imagery technology instruments are implemented on UAVs: RGB, multispectral (MS), thermal infrared (TIR), 3D-radar, visible (VIS), short-wave infrared (SWIR), short-wave near-infrared (SW-NIR) spectroscopy. Recent studies regard vines vigour, water stress, and grapevine diseases. UAV and satellite MS imagery were compared to measure normalised difference vegetation index (NDVI), which is related to crop vigour [5]. MS and RGB airborne remote sensing imagery were adopted to evaluate vines vigour from NDVI and to relate it to yield, berry composition and vine sanitary status [6]. RGB, MS, TIR imagery were implemented to evaluate NDVI, crop surface model (CSM), surface temperature, and crop water stress index (CWSI) [7], [8], with the aim of correlating vigour maps with potential water stress of vines and canopy height to assess climate change impact [7]. Vegetation indexes data (NDVI, green NDVI, red-edge NDVI and normalized difference infrared index) from space-borne and UAV imagery in VIS-NIR-SWIR bands were compared with extracted anatomical and stable isotope traits (linked with hydraulic behaviour, water status and use of resources) from tree-ring series [9]. Aerial SWIR and multispectral UAV data were applied to estimate water stress in vineyards [10]. Merged 3D point cloud, MS and TIR data related to crop canopy were adopted to describe vines vigour and water stress [11]. Airborne TIR imagery was adopted to compare water stress indexes CWSI and linear thermal index (I_g) with the traditional vine water status metrics stomatal conductance (g_s) and stem water potential (Ψ_s) [12]. Airborne MS imagery data were integrated with a decision-oriented vine water consumption model to optimize precision irrigation [13]. 3D point cloud crop models were adopted to describe vineyard 3D macro-structure [14] and to evaluate leaf area index (LAI) [15]. Flavescence dorée grapevine disease [16]–[18] and grape trunk diseases [17] were evaluated by means of MS [16], [17] and RGB [18] imagery.

In recent decades, global climate change has generally led to an increase in the soluble solids content (SSC), or sugar content, of the berries. Usually, harvesting tends to be carried out earlier, phenolic and aromatic ripeness is not always reached, and acidity tends to decrease. As a result, the alcohol content of the wine increases, in contrast to its ageing capacity [19]. However, for instance by acting on irrigation through the use of techniques such as the regulated deficit irrigation (RDI), significant increases in SSC and anthocyanins can be achieved, together with a decrease in yield and berry size,

leading to substantial improvements in grape quality [20], [21].

Monitoring of grape quality attributes can be carried out directly in the field using traditional destructive techniques. Alternatively, quality attributes can be estimated through the use of non-destructive techniques, such as near infrared (NIR) spectroscopy. Portable NIR instruments were used to determine the following quality attributes of grapes: water content, SSC, reductant sugars, pH, titratable acidity (TA), maturity index (sugar/acidity ratio), extractable anthocyanins (EA), potential anthocyanins (PA) [22].

Among the spectroscopic techniques, since a couple of decades the use of hyperspectral imaging (HSI) technology in the quality assessment of fruits and vegetables has become of increasing interest [23], [24]. HSI was initially limited to controlled environments such as laboratories: gradually, thanks to the miniaturization and to the increase in computing and data storage capabilities of the instruments, its use began to spread directly in the field [25]. Hyperspectral (HS) images can be captured either remotely by airborne vehicles and unmanned aerial vehicles [26]–[28], or by ground vehicles [29]–[35], which produce proximal HS images with high spatial resolution. Proximal HSI could therefore allow non-destructive, contactless and automated monitoring of grape quality attributes. Moreover, the acquisition of hyperspectral images can be performed continuously, enabling the rapid scanning of large areas. The HS data is characterized by two spatial and one spectral dimension, therefore only specific regions of interest (ROI) can be selected and the residual regions can be excluded.

The present study aims to predict the SSC of grapes through the use of HSI technology directly in the field, in order to observe the SSC evolution during ripening. Spectral classification on each HS image was achieved by manually selecting the points. To the resulting mean spectrum, absolute difference (Manhattan) metric distance function was applied. From the classified points resulting from each HS image a mean spectrum was calculated. The SSC content in grapes was predicted by means of PLS regression.

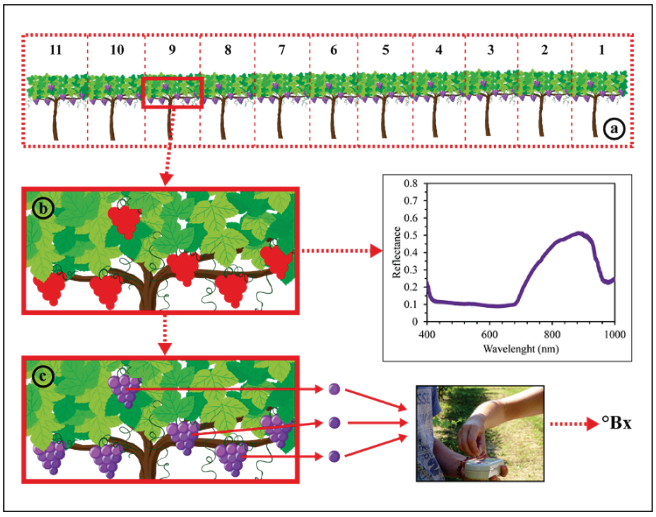

Fig. 1 (a) Representation of the vineyard row analyzed, which was divided into 11 sections. (b) A hyperspectral image was acquired for each section of the vineyard row (section n. 9 is provided for illustrative purposes) for each day of analysis; the mean spectrum of grape berries was calculated, which was obtained by manually selecting 5 zones within the grape berries and then applying the absolute difference Manhattan function. The regions of interest obtained are represented in red. (c) 3 grape berries were collected for each section of the vineyard row (section n. 9 is provided for illustrative purposes) for each day of analysis; soluble solids content, expressed in °Bx, was measured using a digital refractometer; afterwards, the mean value of soluble solids content was calculated.

II. MATERIALS AND METHODS

A. Samples and setup

One side of a row of 'Sangiovese' (*Vitis vinifera* L.) grape vineyards, located near Cesena (Italy), was analyzed on 13 different days in the period between August 20th and October 4th, 2019.

The row was divided into 11 sections; from each section 3 grapes were taken for each day of analysis, for a total of 429 samples (Fig. 1).

B. Hyperspectral scans

The adopted push-broom hyperspectral camera (HSC) (Nano-Hyperspec VNIR, Headwall Photonics, Inc., Fitchburg, MA, USA) scans single lines in a sequence, each one consisting of 640 voxels: the HS image is created by moving the HSC along the scanning direction (Fig. 2). Each voxel contains, in addition to the two spatial dimensions, a

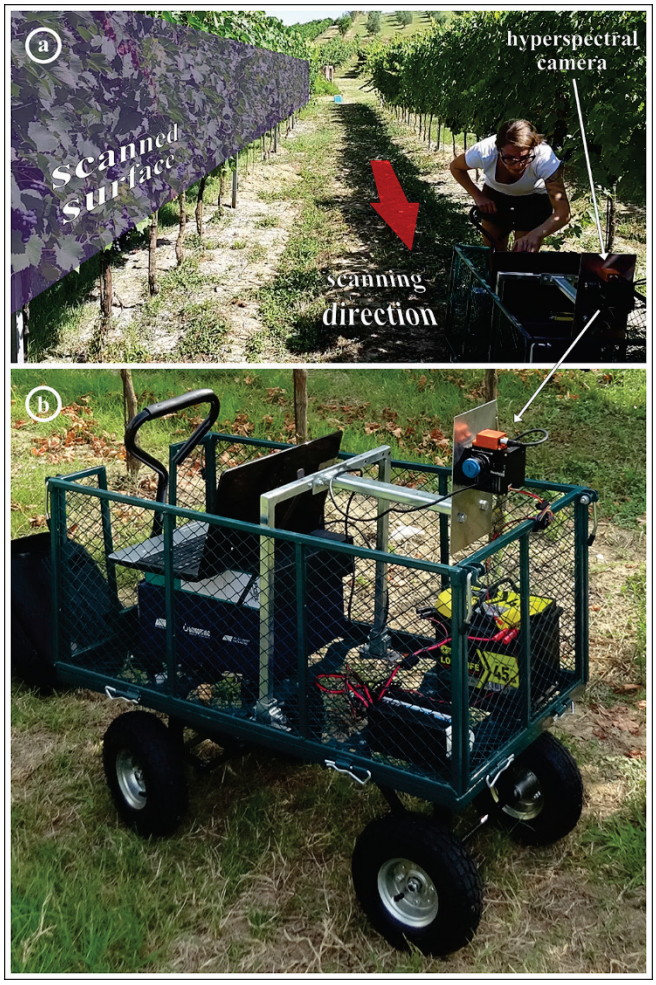

Fig. 2 (a) In-field hyperspectral imaging to measure soluble solids content of wine grape berries during ripening. In the picture a vineyard row, highlighted by the purple surface, was scanned with a Vis/NIR hyperspectral camera: the red arrow indicates the direction of scanning. The vineyard is located near Cesena, Italy. (b) Cart adopted for hyperspectral image acquisition.

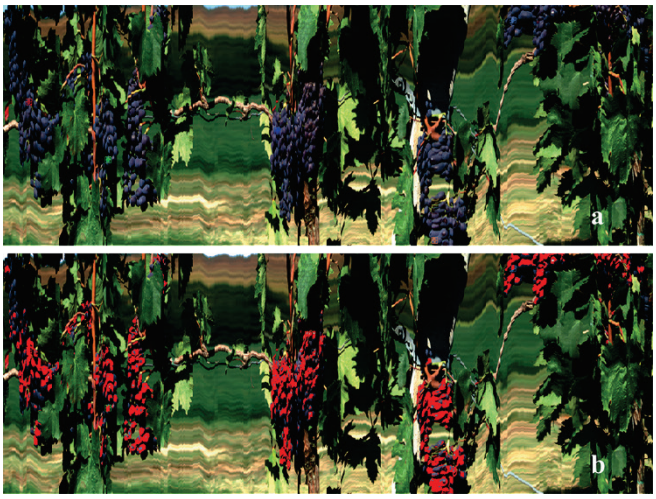

Fig. 3 (a) RGB image from a hyperspectral image of a scanned vineyard row section. (b) Representation of the regions of interest resulting from the classification (in red), from which the mean spectrum of the scanned vineyard row section was derived.

Vis/NIR spectrum (400–1000 nm) characterized by 272 spectral bands, with a nominal spectral resolution of 2.2 nm. The mounted lens has an effective focal length (EFL) of 17 mm, with the optical axis perpendicular to the side of the vineyard row (scanned surface) analyzed. The HSC was installed on a garden cart (Fig. 2) 120 cm above the ground. The scans were performed at about 160 cm from the side of the vineyard row. The HSC was powered by a 12 V, 45 Ah automotive battery through a DC to AC power inverter.

A HS image from each of the 11 sections obtained from the vineyard row was acquired per day of analysis: therefore, during the 13 days of analysis, a total of 143 vineyard row sections were scanned. Direct sunlight in clear sky conditions, from 10:30 to 12:00, was exploited as a light source.

The raw diffuse reflectance spectrum (R_R) was extracted from the HS images.

C. *Destructive measurement of soluble solids content*

After the acquisition of the HS images, the SSC, expressed in °Brix (°Bx), of the grape berries was measured using a portable digital refractometer (PR-101 Digital Refractometer, ATAGO CO., LTD, Tokyo, Japan). From 3 grape berries from each of the 11 sections of the vineyard row, 2 drops of juice per berry were extracted and analysed, and finally the mean for each section was calculated. The SSC measurement was repeated on all days of analysis.

Analysis of variance (ANOVA) with Tukey-HSD post-hoc test (p-level > 0.05) was applied to evaluate significant differences between SSC means over the different days of analysis.

D. *HSI analysis*

Spectra classification was achieved adopting the software HyperCube, v. 11.52 (U.S. Army Engineer Research and Development Center – ERDC, USA). For each HS image, 5 points and a maximum of a further 120 in surrounding neighborhoods (11×11 voxels matrix, with the selected hypercube point in the center of the matrix) were manually selected on 5 different berries directly illuminated by the sun, not in the shade (Fig. 3). Finally, those points (reference) whose metric distance, calculated by applying absolute difference (Manhattan) function and normalized in the range [0,1], from the mean spectrum (signature) of the manually selected points was within the range (tolerance threshold) [0,0.04] were included in the classification (Fig. 3).

From the spectra of the classified points, the mean spectrum for each HS image was calculated.

A PLS regression model (The Unscrambler 9.7, Camo Analytics AS, Oslo, Norway) was developed to estimate the SSC of berries. The spectral bands between 400–424 nm and 976–1000 nm were omitted as a result of the low signal-to-noise ratio (SNR) produced by the HS sensor. The mean spectra were mean-centered and pre-treated with the Savitzky-Golay smoothing transformation (polynomial order:2; smoothing points: 15) and the standard normal variate (SNV) method to reduce noise from the spectra and enhance prediction performance. The validation was carried out by the segmented random cross-validation method (segments: 10).

III. RESULTS AND DISCUSSION

The increase in SSC between the first and last day of analysis was 27.5%, from 17.8 °Bx (day I) to 22.7 °Bx (day XIII). There were significant differences between the SSC values during the investigated period.

Raw mean spectra of all the samples by day of analysis are presented in Fig. 4. In the Vis/NIR region (400–1000 nm), the visible spectrum (400–700 nm) presents the absorption bands of some substances used as ripening indexes of fruit: anthocyanins at around 500 nm, carotenoids at 570–590 nm, and chlorophyll-α at 680–710 nm [36], [37]. In the NIR region (700–1000 nm), absorption bands of water at 760 nm and 960–970 nm are characterized by the overtone of O-H bonds [38], [39]: since the water content of a ripe wine grape is 70–80% [40], it can be expected that the water-related absorption band will prevail. Absorption bands around 840 nm were associated with sugar [41]; moreover, peaks observed in the 950–1000 nm region were related to both water and carbohydrates, as the second overtone of O-H and N-H, a combination band of O-H bonds and the third overtone of C-H, were found in the region [42]. As observed, the water absorption peaks in the NIR (700–1000 nm) spectral region are not very marked and wide. Therefore, spectral information from SSC in the 800–1000 nm range will tend to be less covered by water [42], [43].

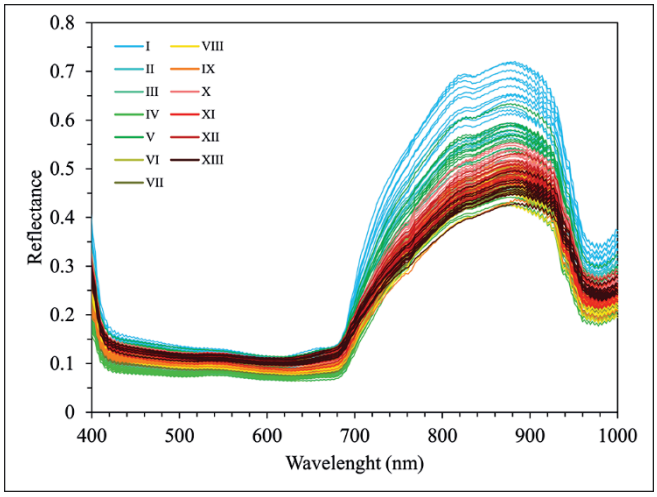

Fig. 4 Raw spectra of all samples on different days (from I to XIII) of analysis.

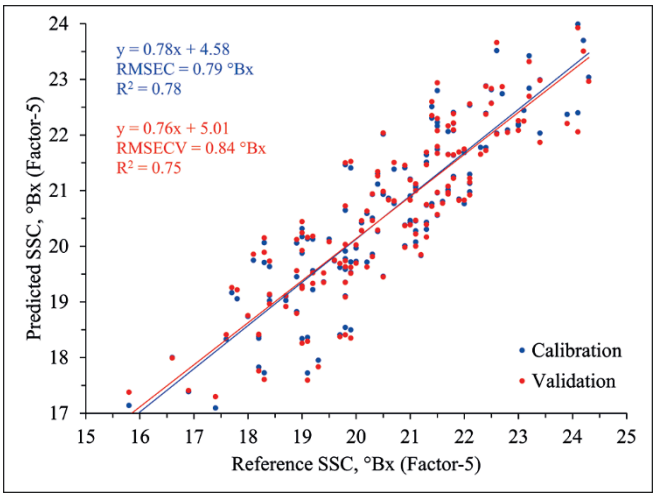

Fig. 5 Reference vs predicted values of soluble solids content (°Bx) in calibration (blue) and cross-validation (red), obtained by PLS regression.

The PLS results, in terms of R^2, RMSE and number of latent variables, in calibration and cross-validation, are reported in (Fig. 5). The model was obtained pre-treating (Savitzky-Golay smoothing, SNV) and mean-centering the spectra; the best predictive power was achieved selecting 5 latent variables. Prediction of grape SSC yielded a $R^2 = 0.75$ in cross-validation (RMSECV = 0.84 Bx).

Other studies developed prediction models employing spectra in the same wavelength range of the present study: Reference [44] adopted a lab-scale HSI system (400–1000 nm) with artificial illumination to analize SSC on seven cultivars of white and red/black table grapes (120 samples), obtaining by PLSR a R^2 of respectively 0.93 and 0.94 in validation, with a RMSE of 0.06 and 0.12 °Bx. Reference [45] predicted SSC on 480 samples of 'Cabernet Sauvignon' wine grape berries with a portable hand-held NIR spectrometer (590–1090 nm), obtaining a $R^2 = 0.72$ and SEPCV = 0.61 °Bx. Reference [46] adopted a Vis/NIR spectrometer (400–1000 nm) directly in the field on 156 grape samples, obtaining in validation $r = 0.82$ and RMSEP = 1.48 °Bx. Considering the r and R^2 values of the above-mentioned studies conducted directly in the field or with portable instruments, it can be found that they are in agreement with the value of the present study.

IV. CONCLUSIONS

Hyperspectral imaging technology, usually adopted in laboratories with auxiliary artificial lighting, in the present study has proved to be suitable to predict directly in the field and under natural lighting conditions the SSC of wine grapes, in order to monitor their evolution during ripening. The development of a predictive model based on PLS produced results similar to those obtained with portable Vis/NIR spectrometers, with $R^2 = 0.75$ and RMSECV = 0.84 °Bx.

The implementation of a hyperspectral imaging system on an agricultural vehicle coupled to a gimbal stabilization system, together with the development of hyperspectral image segmentation techniques, in order to reduce the data size, to select regions of interest and to process spectra, would allow on-the-go analysis of large vineyard extensions. Attention should be paid to the presence of water on the surface of the sample under analysis, to the presence of variable cloudiness and, in case the leaves are analysed, to the presence of wind.

REFERENCES

[1] OIV (International Organisation of Vine and Wine), "2019 Statistical Report on World Vitiviniculture." p. 23, 2019, doi: 64/19/6835 [pii]\n10.1158/0008-5472.CAN-04-1678.

[2] EPRS - European Parliament Research Service, "Precision agriculture and the future of farming in Europe: Scientific foresight study." EPRS, Scientific Foresight Unit (STOA), Brussels, p. 42, 2016, doi: 10.2861/020809.

[3] L. G. Santesteban, "Precision viticulture and advanced analytics. A short review," *Food Chem.*, vol. 279, no. April 2018, pp. 58–62, 2019, doi: 10.1016/j.foodchem.2018.11.140.

[4] A. Matese *et al.*, "Intercomparison of UAV, aircraft and satellite remote sensing platforms for precision viticulture," *Remote Sens.*, vol. 7, no. 3, pp. 2971–2990, 2015, doi: 10.3390/rs70302971.

[5] A. Khaliq, L. Comba, A. Biglia, D. Ricauda Aimonino, M. Chiaberge, and P. Gay, "Comparison of satellite and UAV-based multispectral imagery for vineyard variability assessment," *Remote Sens.*, vol. 11, no. 4, 2019, doi: 10.3390/rs11040436.

[6] M. Ferrer, G. Echeverría, G. Pereyra, G. Gonzalez-Neves, D. Pan, and J. M. Mirás-Avalos, "Mapping vineyard vigor using airborne remote sensing: relations with yield, berry composition and sanitary status under humid climate conditions," *Precis. Agric.*, vol. 21, no. 1, pp. 178–197, 2020, doi: 10.1007/s11119-019-09663-9.

[7] L. Pádua *et al.*, "Vineyard variability analysis through UAV-based vigour maps to assess climate change impacts," *Agronomy*, vol. 9, no. 10, 2019, doi: 10.3390/agronomy9100581.

[8] L. Pádua, T. Adão, A. Sousa, E. Peres, and J. J. Sousa, "Individual Grapevine Analysis in a Multi-Temporal," vol. 2, pp. 1–21, 2020.

[9] N. Damiano *et al.*, "Retrospective Reconstruction of the Ecophysiological Grapevine Behaviour Through the Analysis of Tree-Ring Series to Validate an Approach to Extract Data from Space-Born and UAV Techniques," in *2019 IEEE International Workshop on Metrology for Agriculture and Forestry, MetroAgriFor 2019 - Proceedings*, 2019, pp. 191–195, doi: 10.1109/MetroAgriFor.2019.8909258.

[10] Z. Kandylakis, A. Falagas, C. Karakizi, and K. Karantzalos, "Water Stress Estimation in Vineyards from Aerial SWIR and multispectral UAV data," *Remote Sens.*, vol. 12, no. 15, 2020, doi: 10.3390/RS12152499.

[11] L. Comba, A. Biglia, D. R. Aimonino, P. Barge, C. Tortia, and P. Gay, "2D and 3D data fusion for crop monitoring in precision agriculture," in *2019 IEEE International Workshop on Metrology for Agriculture and Forestry, MetroAgriFor 2019 - Proceedings*, 2019, pp. 62–67, doi: 10.1109/MetroAgriFor.2019.8909219.

[12] V. Pagay and C. M. Kidman, "Evaluating Remotely-Sensed Grapevine (Vitis vinifera L.) Water Stress Responses across a Viticultural Region," *Agronomy*, vol. 9, no. 11, 2019, doi: 10.3390/agronomy9110682.

[13] J. Bellvert, M. Mata, X. Vallverdú, C. Paris, and J. Marsal, "Optimizing precision irrigation of a vineyard to improve water use efficiency and profitability by using a decision-oriented vine water consumption model," *Precis. Agric.*, no. 0123456789, 2020, doi: 10.1007/s11119-020-09718-2.

[14] M. Weiss and F. Baret, "Using 3D Point Clouds Derived from UAV RGB Imagery to Describe Vineyard 3D Macro-Structure," *Remote Sens.*, vol. 9, no. 2, p. 111, 2017, doi: 10.3390/rs9020111.

[15] L. Comba *et al.*, "Leaf Area Index evaluation in vineyards using 3D point clouds from UAV imagery," *Precis. Agric.*, vol. 21, no. 4, pp. 881–896, 2020, doi: 10.1007/s11119-019-09699-x.

[16] J. Albetis *et al.*, "Detection of Flavescence dorée grapevine disease using Unmanned Aerial Vehicle (UAV) multispectral imagery," *Remote Sens.*, vol. 9, no. 4, pp. 1–20, 2017, doi: 10.3390/rs9040308.

[17] J. Albetis *et al.*, "On the potentiality of UAV multispectral imagery to detect Flavescence dorée and Grapevine Trunk Diseases," *Remote Sens.*, vol. 11, no. 1, 2019, doi: 10.3390/rs11010023.

[18] M. A. Musci, C. Persello, and A. M. Lingua, "UAV images and deep-learning algorithms for detecting flavescence doree disease in grapevine orchards," *Int. Arch. Photogramm. Remote Sens. Spat. Inf. Sci. - ISPRS Arch.*, vol. 43, no. B3, pp. 1483–1489, 2020, doi: 10.5194/isprs-archives-XLIII-B3-2020-1483-2020.

[19] S. Delrot, H. Medrano, E. Or, L. Bavaresco, and S. Grando, *Methodologies and results in grapevine research*. Springer Netherlands, 2010.

[20] A. Pellegrino, E. Lebon, T. Simonneau, and J. Wery, "Towards a simple indicator of water stress in grapevine (Vitis vinifera L.) based on the differential sensitivities of vegetative growth components," *Aust. J. Grape Wine Res.*, vol. 11, no. 3, pp. 306–315, 2005, doi: 10.1111/j.1755-0238.2005.tb00030.x.

[21] C. Acevedo-Opazo, S. Ortega-Farias, and S. Fuentes, "Effects of grapevine (Vitis vinifera L.) water status on water consumption, vegetative growth and grape quality: An irrigation scheduling application to achieve regulated deficit irrigation," *Agric. Water Manag.*, vol. 97, no. 7, pp. 956–964, 2010, doi: 10.1016/j.agwat.2010.01.025.

[22] C. A. Teixeira Dos Santos, M. Lopo, R. N. M. J. Páscoa, and J. A. Lopes, "A review on the applications of portable near-infrared spectrometers in the agro-food industry," *Appl. Spectrosc.*, vol. 67, no. 11, pp. 1215–1233, 2013, doi: 10.1366/13-07228.

[23] D. Liu, X. A. Zeng, and D. W. Sun, "Recent Developments and Applications of Hyperspectral Imaging for Quality Evaluation of Agricultural Products: A Review," *Crit. Rev. Food Sci. Nutr.*, vol. 55, no. 12, pp. 1744–1757, 2015, doi: 10.1080/10408398.2013.777020.

[24] I. Chandrasekaran, S. S. Panigrahi, L. Ravikanth, and C. B. Singh, "Potential of Near-Infrared (NIR) Spectroscopy and Hyperspectral Imaging for Quality and Safety Assessment of Fruits: an Overview," *Food Anal. Methods*, vol. 12, no. 11, pp. 2438–2458, 2019, doi: 10.1007/s12161-019-01609-1.

[25] A. Benelli, C. Cevoli, and A. Fabbri, "In-field hyperspectral imaging: An overview on the ground-based applications in agriculture," *J. Agric. Eng.*, vol. LI, no. 1030, pp. 129–139, Sep. 2020, doi: 10.4081/jae.2020.1030.

[26] A. Matese and S. F. Di Gennaro, "Technology in precision viticulture: A state of the art review," *Int. J. Wine Res.*, vol. 7, no. 1, pp. 69–81, 2015, doi: 10.2147/IJWR.S69405.

[27] P. J. Zarco-Tejada, M. L. Guillén-Climent, R. Hernández-Clemente, A. Catalina, M. R. González, and P. Martín, "Estimating leaf carotenoid content in vineyards using high resolution hyperspectral imagery acquired from an unmanned aerial vehicle (UAV)," *Agric. For. Meteorol.*, vol. 171–172, pp. 281–294, 2013, doi: 10.1016/j.agrformet.2012.12.013.

[28] T. Ishida *et al.*, "A novel approach for vegetation classification using UAV-based hyperspectral imaging," *Comput. Electron. Agric.*, vol. 144, no. December 2017, pp. 80–85, 2018, doi: 10.1016/j.compag.2017.11.027.

[29] D. Deery, J. Jimenez-Berni, H. Jones, X. Sirault, and R. Furbank, "Proximal remote sensing buggies and potential applications for field-based phenotyping," *Agronomy*, vol. 4, no. 3, pp. 349–379, 2014, doi: 10.3390/agronomy4030349.

[30] Y. Huang, M. A. Lee, S. J. Thomson, and K. N. Reddy, "Ground-based hyperspectral remote sensing for weed management in crop production," *Int. J. Agric. Biol. Eng.*, vol. 9, no. 2, pp. 98–109, 2016, doi: 10.3965/j.ijabe.20160902.2137.

[31] S. Jay *et al.*, "Estimating leaf chlorophyll content in sugar beet canopies using millimeter- to centimeter-scale reflectance imagery," *Remote Sens. Environ.*, vol. 198, pp. 173–186, 2017, doi: 10.1016/j.rse.2017.06.008.

[32] J. Underwood, A. Wendel, B. Schofield, L. McMurray, and R. Kimber, "Efficient in-field plant phenomics for row-crops with an autonomous ground vehicle," *J. F. Robot.*, vol. 34, no. 6, pp. 1061–1083, 2017, doi: 10.1002/rob.21728.

[33] S. Gutiérrez, J. Fernández-Novales, M. P. Diago, and J. Tardaguila, "On-the-go hyperspectral imaging under field conditions and machine learning for the classification of grapevine varieties," *Front. Plant Sci.*, vol. 9, no. July, pp. 1–11, 2018, doi: 10.3389/fpls.2018.01102.

[34] R. L. Whetton, T. W. Waine, and A. M. Mouazen, "Hyperspectral measurements of yellow rust and fusarium head blight in cereal crops: Part 2: On-line field measurement," *Biosyst. Eng.*, vol. 167, pp. 144–158, 2018, doi: 10.1016/j.biosystemseng.2018.01.004.

[35] A. Wendel, J. Underwood, and K. Walsh, "Maturity estimation of mangoes using hyperspectral imaging from a ground based mobile platform," *Comput. Electron. Agric.*, vol. 155, no. June, pp. 298–313, 2018, doi: 10.1016/j.compag.2018.10.021.

[36] G. ElMasry, N. Wang, A. ElSayed, and M. Ngadi, "Hyperspectral imaging for nondestructive determination of some quality attributes for strawberry," *J. Food Eng.*, vol. 81, no. 1, pp. 98–107, Jul. 2007, doi: 10.1016/j.jfoodeng.2006.10.016.

[37] S. Munera *et al.*, "Astringency assessment of persimmon by hyperspectral imaging," *Postharvest Biol. Technol.*, vol. 125, pp. 35–41, Mar. 2017, doi: 10.1016/j.postharvbio.2016.11.006.

[38] B. M. Nicolaï *et al.*, "Nondestructive measurement of fruit and vegetable quality by means of NIR spectroscopy: A review," *Postharvest Biol. Technol.*, vol. 46, no. 2, pp. 99–118, Nov. 2007, doi: 10.1016/j.postharvbio.2007.06.024.

[39] V. A. McGlone and S. Kawano, "Firmness, dry-matter and soluble-solids assessment of postharvest kiwifruit by NIR spectroscopy," *Postharvest Biol. Technol.*, vol. 13, no. 2, pp. 131–141, Apr. 1998, doi: 10.1016/S0925-5214(98)00007-6.

[40] FAO (Food and Agriculture Organization), "Grapes Wine," *FAO Agribusiness handbook*. p. 49, 2009.

[41] H. Pu, D. Liu, L. Wang, and D. W. Sun, "Soluble Solids Content and pH Prediction and Maturity Discrimination of Lychee Fruits Using Visible and Near Infrared Hyperspectral Imaging," *Food Anal. Methods*, vol. 9, no. 1, pp. 235–244, Jan. 2016, doi: 10.1007/s12161-015-0186-7.

[42] C. Camps and D. Christen, "On-tree follow-up of apricot fruit development using a hand-held NIR instrument," *J. Food, Agric. Environ.*, vol. 7, no. 2, pp. 394–400, 2009.

[43] M. Manley, E. Joubert, L. Myburgh, E. Lotz, and M. Kidd, "Prediction of soluble solids content and post-storage internal quality of Bulida apricots using near infrared spectroscopy," *J. Near Infrared Spectrosc.*, vol. 15, no. 3, pp. 179–188, 2007, doi: 10.1255/jnirs.725.

[44] A. Baiano, C. Terracone, G. Peri, and R. Romaniello, "Application of hyperspectral imaging for prediction of physico-chemical and sensory characteristics of table grapes," *Comput. Electron. Agric.*, vol. 87, pp. 142–151, Sep. 2012, doi: 10.1016/j.compag.2012.06.002.

[45] B. Diezma-Iglesias, P. Barreiro, R. Blanco, and F. J. García-Ramos, "Comparison of robust modeling techniques on NIR spectra used to estimate grape quality," in *Acta Horticulturae*, 2008, vol. 802, pp. 367–372, doi: 10.17660/ActaHortic.2008.802.48.

[46] R. Guidetti, R. Beghi, and L. Bodria, "Evaluation of grape quality parameters by a simple VIS/NIR system," *Trans. ASABE*, vol. 53, no. 2, pp. 477–484, Mar. 2010.